

# A 2D inverse problem of predicting boiling heat transfer in a long fin

Tadeusz Orzechowski<sup>1</sup>

Received: 6 May 2015 / Accepted: 23 November 2015 / Published online: 9 December 2015  
© The Author(s) 2015. This article is published with open access at Springerlink.com

**Abstract** A method for the determination of local values of the heat transfer coefficient on non-isothermal surfaces was analyzed on the example of a long smooth-surfaced fin made of aluminium. On the basis of the experimental data, two cases were taken into consideration: one-dimensional model for  $Bi < 0.1$  and two-dimensional model for thicker elements. In the case when the drop in temperature over the thickness could be omitted, the rejected local values of heat fluxes were calculated from the integral of the equation describing temperature distribution on the fin. The corresponding boiling curve was plotted on the basis of temperature gradient distribution as a function of superheat. For thicker specimens, where  $Bi > 0.1$ , the problem was modelled using a 2-D heat conduction equation, for which the boundary conditions were posed on the surface observed with a thermovision camera. The ill-conditioned inverse problem was solved using a method of heat polynomials, which required validation.

## List of symbols

$A, B$	Matrices
$a_i$	Coefficients
$Bi$	Biot number
$b_i$	Coefficients
$C$	Vector
$C$	Integration constant
$c_j$	Coefficients
$F$	Cross-sectional area

$f$	Generating function
$I$	Error functional
$L$	Fin length
$M$	Total number of measured points
$N$	Degree of the polynomial approximating the exact solution
$P$	Perimeter of the fin cross-section
$p$	Parameter
$Q_b$	Total heat conducted at the base of the fin
$q$	Heat flux
$q_\alpha$	Boiling heat flux
$SD$	Standard deviation
$u, w$	Polynomials
$V_j$	Sequence of harmonic polynomials
$x, y$	Coordinates
$x_m$	Coordinate of experimental points

## Greeks

$\alpha$	Heat transfer coefficient
$\lambda$	Thermal conductivity
$\theta$	Wall superheat
$\theta_b$	Wall superheat at the fin's base
$\Theta$	Wall superheat approximation

## 1 Introduction

Heat transfer in the nucleate boiling regime, especially the heat flux density, has been a subject of interest since the 1950s. Although much research has been devoted to the problem, no satisfactory explanation of the physical phenomena accompanying the process has been found. That is mainly due to the fact that the physics of mass, momentum and energy transfer between the surface of the solid body and the wetting fluid is difficult to explain and describe.

✉ Tadeusz Orzechowski  
todek@tu.kielce.pl

<sup>1</sup> Environmental Engineering Department, EcoClimatica Association, Kielce University of Technology, Aleja Tysiąclecia Państwa Polskiego 7, 25-314 Kielce, Poland

Another reason is the nucleation, growth and detachment of vapour bubbles, which, at appropriately high wall superheat, lead to a crisis called the first critical point.

A wide review of physical models describing the boiling process and a means of predicting the operation of smooth surface heat exchangers were presented by Dhir [1]. In the last 80 years, a number of empirical and mechanism based correlations have been proposed for nucleate pool boiling. Empirical correlations differ from each other substantially with respect to the functional form of the heat flux density depending on fluid and surface properties. Additionally, all of them require knowledge of the density of active sites, bubble diameter, its frequency of departure, etc. However, because of the complex nature of the coexisting processes, it has not been possible to develop comprehensive formulas for these parameters.

The experimental data concerning boiling heat transfer described in the literature focus on isothermal surfaces. This is primarily due to the measuring technique, which involves mounting a specimen on the heating element. The power is determined directly by measuring the electricity supplied, as done by Ahn et al. [2, 3] and Naphon et al. [4], or indirectly by applying a gradient method including measurement of temperature at several points along the specimen axis, as done by Ahn et al. [5]. The final result of the experiment is a boiling curve, which shows the relationship between the heat flux density and the heat transfer coefficient as a function of wall superheat. The generalized results are illustrated in the form of correlations for the Nusselt number.

In the case of nucleate boiling heat transfer on smooth surfaces, the Rohsenow equation is used, and values of the required constants are selected for various surface-fluid combinations, Pioro [6] and Pioro et al. [7]. The factors involved in boiling heat transfer include the type, state, shape and orientation of the surface, the type of the fluid, possibly the amount of foreign particles, etc. However, the correlation relationships determined by different researchers even under the same or similar geometric and material conditions will differ. For instance, Kolev [8] analyzes a number of different correlation equations describing heat transfer for water boiling at ambient pressure on smooth surfaces. The values of the heat flux density calculated by means of these relationships differ, which can be explained by the fact that the measurements were conducted under different conditions and the surfaces differed in state. Sixteen different correlations to predict the boiling heat transfer coefficient are analyzed and compared to evaluate their use in evaporator design by Adib and Vasseur [9]. From this review, it appears that it is difficult to predict the proper value of the heat flux on the basis of the existing formulas found in the literature. A large number of correlations available in the literature are seldom satisfactory. Using

the available literature and experimental test results, some researchers try to find a universal correlation for the boiling heat transfer coefficients, as Shah [10]. Although they make progress in prediction accuracy, so far such attempts are still not satisfactory for general purposes.

Physical phenomena accompanying nucleate boiling are also considered theoretically. A 2D numerical investigation of boiling with a energy balance simulation is applied by Orzechowski et al. [11]. Measured and numerically calculated values of heat transfer coefficient demonstrate good congruence, which indicates a correct selection of measurement methods and a cogent analysis of the experimental results. The application of the heat transfer theory to pool boiling is discussed by Roh [12]. The study provides an explicit illustration of the kinetics of phase transition mechanisms at the interface of two different phase materials.

Considerable divergence of results discussed in the literature indicates that the designed heat transfer elements should be measured separately. This is particularly essential in the case of non-isothermal surfaces, where the boiling heat transfer processes differ significantly from those observed on surfaces with uniformly distributed temperature, as shown by Orzechowski [13]. A typical example, discussed by Krikkis [14], Liaw et al. [15] and Gonzalez-Fernandez et al. [16], is a fin, on the surface of which different boiling regimes can be distinguished. Similar conclusions are sought analytically by Turkyilmazoglu [17] and Kundu et al. [18]. They determine the performance of different fin geometries by analyzing the temperature-dependent thermal conductivity of the fin material, the variable heat transfer coefficient under different boiling regimes or surface conditions. A original technique for determining the transient heat transfer coefficients from measured temperatures inside solids is presented in [19]. Numerical examples are given as verification of the method.

Maintaining the heat transfer rate and the desired operating temperature is an important task when a reliable operation of machinery components is to be provided. The proper design of the heat exchangers can produce an efficient solution to the problem. Chen et al. [20] applied an inverse method together with FLUENT software and the experimental temperature distribution to investigate the non-uniform heat transfer coefficient on the fin in the heat sink for various fin spacings. Torabi and Aziz [21] investigated the thermal performance of T-shaped fins. They accounted for temperature-dependent thermal conductivity, surface emissivity, convection heat transfer coefficient, and non-zero convection and radiation sink temperatures. The problem was solved numerically. Konda Reddy et al. [22] presented a methodology for the estimation of temperature-dependent heat transfer coefficient for a vertical rectangular fin operating in a steady state under natural convection regime. Heat transfer coefficient was considered as a power

law function of temperature excess. Thermal performance of variable diameter micro-pin fins was calculated by Diez et al. [23]. On the basis of an exact solution of smooth pin fins for three selected profiles (hyperbolic, trapezoidal and concave parabolic ones), the approximate series solution was given. The effect of surface roughness on efficiency increase was evaluated. Three different types of fins made of aluminium and copper, at a fixed fin array volume were discussed by Huang et al. [24] while looking for the most efficient solutions to heat sinks. Results obtained by using the Levenberge-Marquardt method to solve 3-D inverse problem were based on the numerical experiments. Estimation of unknown parameters in a rectangular fin satisfying a predefined temperature are discussed by Das et al. [25]. The study is useful for selecting various unknowns in a conductive-convective and radiative fin for required temperature and efficiency.

Grysa et al. [26] presented an approximate method of solving nonlinear inverse stationary heat conduction identification of boundary condition. The obtained results were compared with the direct solution of the problem. A numerical study of the inverse problem of determining time-variable surface heat flux in a plane wall, with constant or temperature dependent thermal properties, is given by Zueco et al. [27]. Direct and inverse heat conduction problems are solved with the network simulation method. Both the accuracy and effectiveness of the method has been discussed.

Considerations such as those mentioned above, aim to determine the performance and optimum design of fin assemblies. The aim of this study was to derive an efficient algorithm for the determination of local values of the boiling heat transfer coefficient using a specimen made of aluminium.

## 2 Experimental procedure and measurements

Investigations were conducted at the test facility, specially arranged for the task. The diagram of the facility is presented in Fig. 1.

The experiment involved a long fin-shaped specimen with a width of 12 mm, an active length of 90 mm and a different thickness, which was placed between two textolite plates. One of the specimen surfaces was in contact with the boiling fluid, and the other was surrounded by quiescent atmospheric air. The test facility was equipped with two independent heating systems. The main heating element, whose power was controlled with an autotransformer, was located at the fin base. The auxiliary heating system, made of spirally coiled resistance wire, was positioned on the bottom of the vessel. A constant supply of the electric power to the auxiliary system was maintained throughout all measurement series. The task of the auxiliary system was to

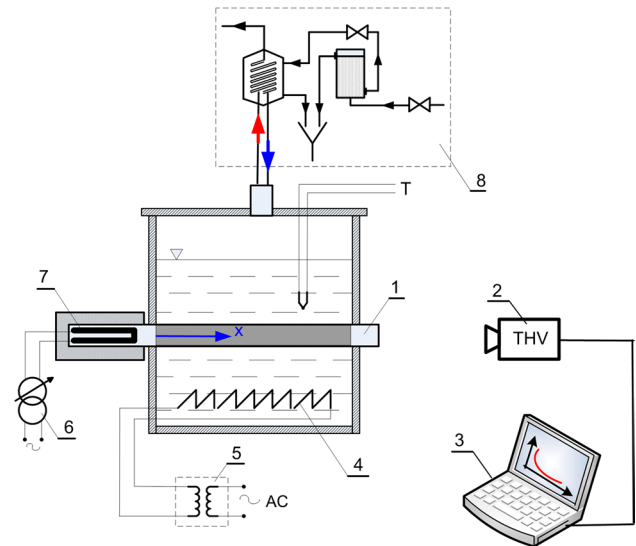


**Fig. 1** Diagram of the test facility for non-isothermal specimens: 1 examined element, 2 thermovision camera, 3 data acquisition system, 4 auxiliary heater, 5 separation system with the control of supplied electric power, 6 autotransformer with the electric power measurement, 7 main heater, 8 cooling and condensate recovery system,  $T$  thermocouple

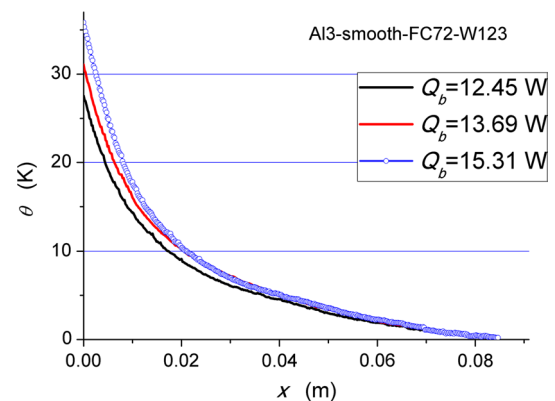


**Fig. 2** Axial temperature distribution for a 3 mm thick smooth aluminium fin

sustain the boiling process in the whole volume of the liquid. Supplying power to the auxiliary system was preceded by a measurement intended to examine the effect produced by the power supply on the results of investigations. Within the whole range of the power supply, no such effect was observed. The test facility was equipped with a cooling and condensate recovery system. Vapours of the boiling liquid condensed in the system of two tap water-cooled condensers, and then flowed, by gravity, into the vessel.

The outer surface of the examined element was observed with a thermal imaging camera, as shown in Fig. 2. Since high emissivity of the observed surface is required to reduce

the uncertainty of the IR temperature measurement, the outer surface was coated in black paint. The optical homogeneity of the observed surface and the emission coefficient in the camera spectral range were determined during the initial calibration process. The experiments were performed using a VIGO System V50 camera, operating in the long-wave infrared range (8–11  $\mu\text{m}$ ), equipped with a  $384 \times 288$  microbolometer FPA (Focal Plane Array), whose sensitivity at a temperature of 30  $^{\circ}\text{C}$  is  $<0.08$  K. The main heater was mounted at the base of the specimen, where the pre-determined time-invariant electric power was supplied. The heater outer surface was shielded so that the emitted radiation would not affect the temperature measurement. The tests were conducted for refrigerant FC 72 at ambient pressure, which after evaporation was directed onto the cooling system in order to recover the condensate. The specimen had to be adequately fixed so that the temperature field observed with the thermal imaging camera could be treated as a one-dimensional quantity. The result of the measurement was the distribution of temperature along the length for the central line of the fin. The test was carried out during refrigerant FC 72 boiling at ambient pressure on a non-isothermal smooth surface of an aluminium fin. Exemplary measurement results for a smooth surface specimen 3 mm in thickness are shown in Fig. 2. The results were obtained for three different heating powers supplied to the fin base.

Measurements of the electrical power applied to the main heater do not reflect the heat dissipated by the fin. It is thus difficult to estimate the amount of heat lost to the surroundings. Moreover, the changes are uneven as they are dependent on the changes in load. It can be assumed that for sufficiently thin specimens the Biot number is small, i.e.  $Bi < 0.1$ , since there is no change in temperature with thickness, it can be omitted and the total heat conducted at the base of the fin  $Q_b$  can be calculated using Fourier's law. The necessary temperature gradient can be determined from the measurement data shown in Fig. 2.

The same experimental set-up was used for a 12 mm thick smooth specimen made of aluminium. It had identical chemical composition and surface morphology as the 3 mm specimen. The electrical power supplied to the main heater was adjusted to keep the temperature of the outer surface at the fin base as close as possible to that reported for the thinner sample. Figure 3 shows the axial temperature distributions in the two fins.

Direct observation of the boiling process at the fin surface shows that for the two samples heat transfer at the base occurs in the fully developed nucleate boiling regime in the vicinity of the critical point. The heat transfer coefficient for nucleate boiling is frequently described by the Rohsenow correlation, which indicates its exponential dependence on the wall superheat [6]. In this case, the total amount of heat dissipated by the fin with a constant cross-section is

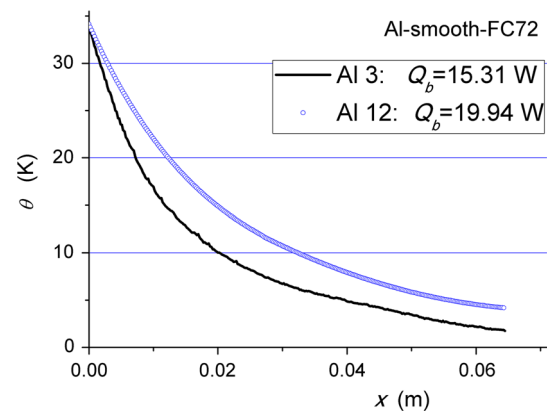


**Fig. 3** Temperature distribution along the centerline of aluminium fins of different thickness

proportional to the square root of the surface at the base, i.e.  $Q_b \sim \sqrt{F_b}$  (see Ref. [28]). The heat transfer surfaces of both fins are of equal dimensions, have the same spatial orientation and morphology, and fins differ only in thickness. With the assumption of constant temperature in the fin cross-section, the amount of heat dissipated by the 12 mm thick fin should be twice as high as the amount of heat dissipated by the 3 mm thick fin. Thus, according to Fourier's law, the derivative of the temperature at the base should be twice as small as that for the thicker fin. However, the values measured were different; they were  $-2412.8$  and  $-1519.1$  K/m for the thinner and thicker fins, respectively, while their ratio was 0.63. This large discrepancy indicates that the 1-D analysis cannot be used for fins with a relatively large thickness. Thus, the problem must be solved numerically.

### 3 Problem formulation and the method of solution

The distribution of temperature on the outer surface measured with the thermovision camera is the evidence of the heat transfer taking place on the surface invisible to the camera. As shown in Fig. 3 the surface temperature distributions along the centrelines of fins of 3 and 12 mm, however, are not the same, which results only from different thicknesses of the samples. The different slopes of the temperature distribution for both specimens indicate that a thicker specimen does not satisfy the Biot number condition and 1-D approximation cannot be applied automatically.

#### 3.1 One-dimensional inverse problem

The method for determining a local value of the heat transfer coefficient over a non-isothermal fin surface can be used only with one-dimensional systems, i.e. ones where the drop in temperature over the thickness can be omitted. This

assumption is true for numbers  $Bi < 0.1$ . At nucleate boiling regime, for extended surfaces, the heat transfer coefficients reach values even higher than  $0.1 \text{ MW/m}^2\text{K}$ . Thus, using a one-dimensional model is possible only for elements with a small thickness that are made of high thermal conductivity materials. For such large values of heat transfer coefficients, a copper fin  $< 0.4 \text{ mm}$  in thickness is required to strictly satisfy the Biot number criterion. Boiling heat transfer of FC72 on the smooth surface of the aluminium sample requires that the sample thickness should be a little below  $4 \text{ mm}$ .

The performance of a straight fin with a constant cross-section is analysed on the basis of one-dimensional expression for the temperature distribution:

$$\frac{d^2\theta}{dx^2} = m_1^2 q_\alpha = m_1^2 \alpha \theta, \quad (1)$$

where  $m_1^2 = P/\lambda F$ , with  $P$  denoting the perimeter of the fin cross-section and  $F$  the cross-sectional area,  $\lambda$  thermal conductivity,  $q_\alpha$  local value of the heat flux rejected by the fin lateral side,  $\alpha$  heat transfer coefficient.

In inverse problems, the temperature distribution is also used to determine the heat transfer coefficient and the heat flux density. The right-hand side of Eq. 1 is dependent only on the wall superheat. Thus, the integration gives

$$\left(\frac{d\theta}{dx}\right)^2 = 2m_1^2 \int q_\alpha d\theta + C = b_0 + b_1\theta + b_2\theta^2 + b_3\theta^3 + b_4\theta^4 + \dots \quad (2)$$

where  $C$  is an integration constant calculated, if necessary, from the boundary condition.

Assuming that the result of integration of the right-hand side of Eq. (2) is described by the holomorphic function, its value can be represented by a power series as shown in (2).

Differentiation of both sides of Eq. (2) is replaced by the following expression for the heat flux density:

$$q_\alpha = \frac{1}{2m_1^2} (b_1 + 2b_2\theta + 3b_3\theta^2 + 4b_4\theta^3 + \dots) \quad (3)$$

where  $m_1^2$  is defined in Eq. (1) while coefficients  $b_i$  result from polynomial fit (see Fig. 5).

### 3.2 Formulation and solution of a 2-D ill-posed problem

In the case of thicker fins, where the differences in temperature between the outer and inner surfaces are large, the assumption of a one-dimensional model leads to considerable errors. A good solution is to apply a method of non-invasive measurement to determine the temperature field on the accessible surface and calculate the heat transfer surface

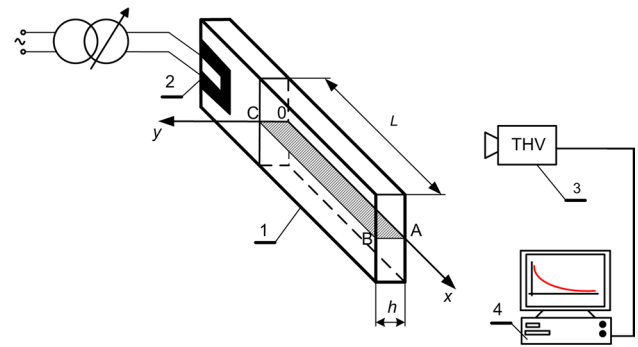


**Fig. 4** View of the element measured: 1 fin, 2 main heater, 3 thermovision camera, 4 data acquisition and processing station,  $L$ ,  $h$  length and thickness of the measured section, respectively

area. Then, the local values of the heat transfer coefficient and heat flux are established.

The conditions of the measurement described above require that the heat transfer coefficients should be determined on the basis of at least the two-dimensional Laplace equation for OABC area shown in Fig. 4.

Two of the boundary conditions on the side observed by the thermovision camera, i.e. the temperature distribution and the dissipated heat flux, are generally easy to estimate. The other boundary conditions need to be determined individually. Thus, that constitutes not only an inverse but also an ill-posed problem. The problem described in this study was solved using heat harmonic polynomials (sometimes called heat polynomials). This method, proposed by Ciałkowski et al. [29], makes it necessary to find an exact solution in the form of an approximation satisfying the two-dimensional heat conduction equation and approximately satisfying the boundary conditions.

For a fin operating in the system presented in Fig. 4, the modelling was based on the stationary two-dimensional heat conduction equation,

$$\frac{\partial^2\theta}{\partial x^2} + \frac{\partial^2\theta}{\partial y^2} = 0 \quad (4)$$

$\theta$  the wall superheat.

It is expected that the solution to  $\theta(x,y)$  should be looked for in the OABC area. Heat is removed from the side surface, BC, at pool boiling of the surrounding medium. The aim of the calculations is to determine some local values of the heat flux density of this energy. The four boundary conditions required to solve the problem are:

- for the thermovision camera OA side (see Fig. 4):

$$\theta(x_m, 0) = f(x_m) \quad (5)$$



$$\frac{\partial \theta}{\partial y} = 0 \quad (6)$$

where  $x_m$  is the coordinate of the experimental points. Condition (5) represents the distribution of discrete surface temperature measured along the central line of the fin, OA, at  $M$  points with the  $x_m$  coordinates. Additionally, it is assumed that the heat flux rejected to the surroundings along OA is negligible in comparison with the flux generated from the BC surface. The phenomenon of boiling heat transfer is observed along the BC side of the fin, while the OA edge is in contact with quiescent atmospheric air. The heat transfer coefficient is several orders of magnitude lower for OA in comparison with BC. The estimations show that for refrigerant boiling at atmospheric pressure the heat flux dissipated by OA is <1 % of the heat flux dissipated by BC, which confirms the correctness of assumption (6). Moreover, it is a condition of the fin central symmetry.

- The temperature distribution in the fin cross-section at the base, OC, is assumed to be constant:

$$\theta(0, y) = \theta_b = \text{const.} \quad (7)$$

- For the fin top (the AB side in Fig. 4), it is assumed that:

$$\frac{\partial \theta(L, y)}{\partial x} = 0 \quad (8)$$

where  $\theta_b$  is the wall superheat at the fin base.

Satisfying condition (8) requires using a fin with a sufficient length,  $L$ . It should be noted that the condition on the BC side is not known, whereas for  $y = 0$ , two conditions are given.

The problem analyzed here is not only inverse but also ill-posed. To solve it, a method of resolving functions (in this case, some kind of polynomials for the local temperature) needs to be employed. For a given differential equation, it is always necessary to determine a generating function dependent on the parameter  $p$ . In accordance with [29], the following function was used:

$$f = e^{p(x+iy)}, \quad \text{where } p \in R \quad (9)$$

because it satisfies the differential Eq. (4).

The coefficients of the Taylor series expansion of the above function relative to the parameter  $p$  are the desired polynomials solving the differential equation. The series expansion of the exponential function (9) is given by the following formula:

$$e^{p(x+iy)} = \sum_{j=0}^{\infty} (x+iy)^j \frac{p^j}{j!} \quad (10)$$

This gives two sequences of harmonic polynomials, the so-called heat polynomials, one being a real part and the other an imaginary part of the complex function,  $(x+iy)^j$ :

$$\begin{aligned} u_j(x, y) &= \text{Re}[(x+iy)^j] \\ w_j(x, y) &= \text{Im}[(x+iy)^j] \end{aligned} \quad (11)$$

The same order polynomials  $u$  and  $w$  are used interchangeably to obtain a sequence of harmonic polynomials  $V_j$ , each of which satisfies the Laplace equation and can be treated as a particular solution of Eq. (4):

$$\begin{aligned} V_0 &= u_0 = 1 \\ V_1 &= u_1 = x \\ V_2 &= w_1 = y \\ V_3 &= u_2 = x^2 - y^2 \\ V_4 &= w_2 = 2xy \\ V_5 &= u_3 = x^3 - 3xy^2 \\ V_6 &= w_3 = 3x^2y - y^3 \\ &\dots \end{aligned} \quad (12)$$

Its general solution is approximated by means of a linear combination of the heat polynomials, which constitute the approximation  $\Theta(x, y)$  of the exact solution having the form of:

$$\begin{aligned} \theta(x, y) &\approx \Theta(x, y) = \sum_{j=0}^N c_j \cdot V_j(x, y) \\ &= c_0 + \sum_{j=0}^{N/2} c_{2j+1} (x \cdot u_{2j} - y \cdot w_{2j}) \\ &\quad + \sum_{j=0}^{N/2-1} c_{2j+2} (x \cdot w_{j+1} + y \cdot u_{j+1}) \end{aligned} \quad (13)$$

$c_j$  coefficients,  $N$  degree of the polynomial approximating the exact solution.

Expression (13) satisfies the Laplace Eq. (4); in a general case, however, it does not exactly satisfy the boundary conditions. One can only demand that the acceptable error be as negligible as possible. The condition assumed in this way allows us to select unknown coefficients  $c_j$ . It is thus essential to express the error functional as:

$$\begin{aligned} I &= \frac{1}{M \cdot \theta_b^2} \sum_{m=1}^M [\Theta(x_m, 0) - f(x_m)]^2 + \frac{L}{\theta_b^2} \int_0^L \left[ \frac{\partial \Theta(x, 0)}{\partial y} \right]^2 dx \\ &\quad + \frac{1}{L \cdot \theta_b^2} \int_0^h [\Theta(0, y) - \theta_b]^2 dy + \frac{L}{\theta_b^2} \int_0^h \left[ \frac{\partial \Theta(L, y)}{\partial x} \right]^2 dy \rightarrow \min \end{aligned} \quad (14)$$

where  $M$  is the total number of measured points. The following terms of the above error functional refer to the differences in boundary conditions (5)–(8) and value of function (13) which represents the approximation of the exact solution of Laplace Eq. (4). All components required in the above expression should be determined from the assumed form of the approximation (13). Then, by differentiating functional (14) in relation to all coefficients  $c_j$ , the following system of linear equations is obtained:

$$\frac{\partial I}{\partial c_i} = 0 \quad \text{for } i = 0, 2, 3, \dots, N \quad (15)$$

Thus, the problem is solved by applying the  $N + 1$  linear equation systems with unknown values of vector  $C = C[c_1, c_2, \dots, c_N]$  with unknown coefficients  $c_j$ :

$$A \cdot C = B \quad (16)$$

where

$$A = \begin{bmatrix} a_{1,1} & \dots & a_{1,N} \\ & \ddots & \\ & & a_{i,j} & \ddots \\ a_{N,1} & & & a_{N,N} \end{bmatrix}, \quad B = \begin{bmatrix} b_1 \\ \vdots \\ b_j \\ \vdots \\ b_N \end{bmatrix} \quad (17)$$

The elements of matrices  $A$  and  $B$  are defined by the following formulae:

$$\begin{aligned} a_{ij} &= \frac{1}{M} \sum_{m=1}^M V_j(x_m, 0) V_i(x_m, 0) + L \int_0^L \frac{\partial V_j(x, 0)}{\partial y} \frac{\partial V_i(x, 0)}{\partial y} dx \\ &\quad + \frac{1}{L} \int_0^h V_j(0, y) V_i(0, y) dy + L \int_0^h \frac{\partial V_j(L, y)}{\partial x} \frac{\partial V_i(L, y)}{\partial x} dy = 0 \\ b_i &= \frac{1}{M} \sum_{m=1}^M f(x_m) V_i(x_m, 0) + \frac{1}{L} \int_0^h \theta_b V_i(0, y) dy \end{aligned} \quad (18)$$

As a result, the desired coefficients of the linear combination of functions (12) are obtained, which, introduced in Eq. (13), form an approximation of the exact solution. By using the obtained relationships, the thermal field in the analyzed area can be determined.

#### 4 Method validation

The temperature measured on the outer surface OA (see Fig. 4) provides information on the processes occurring on the inner surface of the fin, not accessible to the thermovision camera. As a result, the temperature measured is different from the actual one occurring during intensive heat transfer.

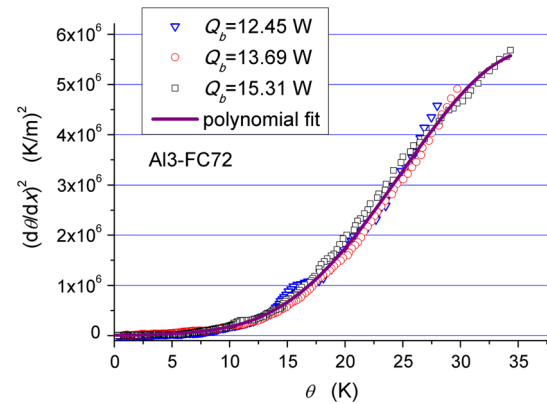


**Fig. 5** Square of the temperature gradient versus wall superheat

The thermal field on the fin surface is measured at many points with a thermovision camera. That makes it possible to apply typical procedures of smoothing and then numerical differentiation available in a number of calculation packages. For the 3 mm thick aluminium fin, the results of the analysis of the measurement data from Fig. 2 are shown in Fig. 5.

Using the polynomial approximation to the data given in Fig. 5, all coefficients of Eq. (2) could be determined and then the local heat fluxes  $q_\alpha$  and heat transfer coefficients could also be established. The corresponding boiling curve for the investigated surface is drawn in Fig. 7. Here and hereafter, the boiling curve is defined locally, i.e. for the local values of heat flux and heat transfer coefficients from superheat. Detailed analysis of the method and its uncertainties are discussed by Orzechowski [28].

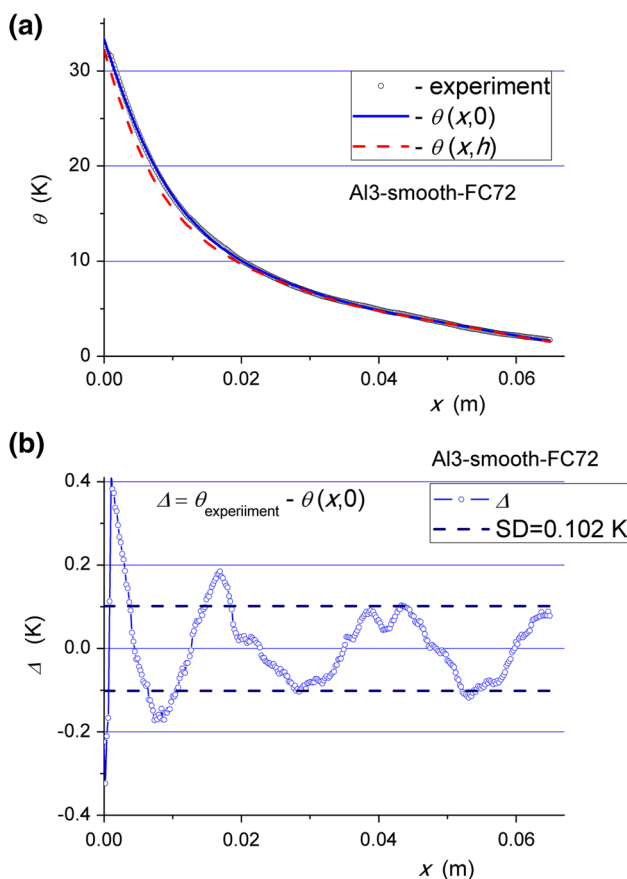
The major factor affecting the proper determination of the heat flux density is the limited accuracy of the measuring device. The smaller are the differences between the temperature values, the greater effect of the measurement accuracy is noted. In this study, a regime around the critical heat flux and free convection boiling was analyzed. The determination of the heat flux density or heat transfer coefficient from error-prone measurement data is very difficult and requires validation of the method, especially if the problems are ill-posed.

The correctness of the developed algorithm is generally verified by a numerical experiment, in which a similar problem is solved analytically. A more reliable method should use, if possible, the experimental data. For that reason, an additional independent test was conducted at the same test facility using the same devices and under the same conditions. The experiments involved measuring the distribution of temperature on the aluminium specimen with a thickness of 3 mm. For aluminium, whose conductivity is very high, and, for the small thickness of the specimen, the condition  $Bi < 0.1$  was well satisfied nearly over

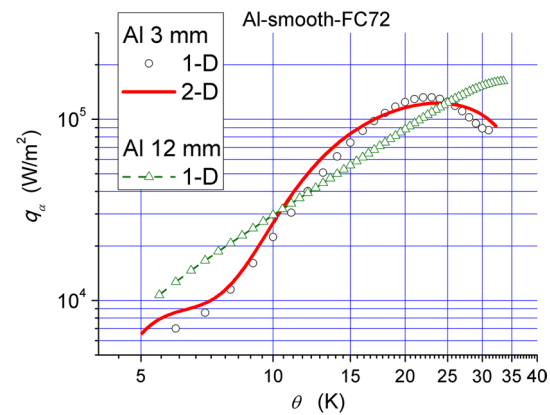
the entire wall superheat range, and the heat transfer could be treated as a one-dimensional problem. The boiling curve was plotted using the method described in Sect. 3, and the results were compared with analogous data using the proposed method of heat polynomials.

Figure 6 shows the temperature measured on the outer surface of the aluminium fin and the temperature calculated for the inverse ill-posed problem using the method of heat polynomials with the boundary conditions (5)–(8). In Fig. 6b, a difference in the measured and calculated temperature is shown. Its mean value is close to zero, and nearly all points are located in the range  $\pm 0.2$  K. Only a few points are positioned outside that range. The probable reason is the local change in the emissivity of the paint, but even with this, the standard deviation for this set is low and equals 0.102 K.

The proposed numerical method used to solve the inverse problem allows us, for instance, to determine the surface temperature and the local heat flux as seen in Fig. 7 as the function of wall superheat in FC-72 boiling on the



**Fig. 6** Results obtained for a 3 mm thick aluminium fin: **a** measured and calculated wall superheats at the outer OA and inner CB lines (see Fig. 4),  $\theta(x,0)$  and  $\theta(x,h)$  respectively, **b** temperature differences between the measured and calculated points at the surface viewed through a thermovision camera ( $y = 0$ )



**Fig. 7** Measured and calculated heat flux for a thin aluminium fin

aluminium fin at ambient pressure. For the sake of comparison, a similar relationship devised using a 1-D model is shown. It is also worth noting that in this particular range, the maximum  $Bi \approx 0.08$  is found at the wall superheat  $\sim 20$  K. As can be seen from the two figures above, the good convergence of the calculation results obtained with two different methods using the same experimental data confirms that the method proposed for solving the ill-conditioned inverse problem is correct.

Similarly, the relationship between the local heat flux removed from the surface and the wall superheat is determined from the distribution of temperature measured at the outer surface of the 12 mm fin, according to the 1-D procedure. This leads to an exponential dependence of  $q$  on  $\theta$ , as shown by the straight line in Fig. 7. The constant exponent can then be determined from its slope. The exponent value 1.52 indicates the presence of only nucleate boiling on the whole fin surface. Moreover, this exponent is twice as small as that given in the Rohsenow correlation [6].

The boiling curves plotted for the two specimens in accordance with the 1-D procedure differ in shape and value. This falsely suggests that the physical phenomena present during the phase change heat transfer differ for the two specimens made of the same material and having the same surface morphology. Since this is not true, proper determination of the boiling heat transfer processes in thick fins requires using a numerical method, which, even for ill-posed problems, gives correct results.

## 5 Discussion

The local values of heat flux density derived in Sect. 4 can be used to calculate the heat transfer coefficient for each wall superheat. As its maximum value is about  $4800 \text{ W/m}^2\text{K}$ , the Biot number for the 3 mm thick fin is smaller than 0.1. For a fin with the same physical parameters but



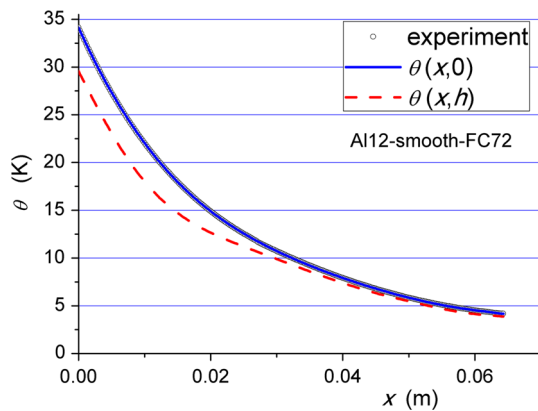
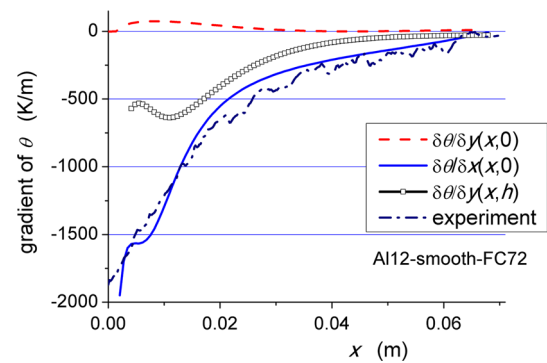


**Fig. 8** Measured and calculated wall superheat for a 12 mm thick aluminium fin

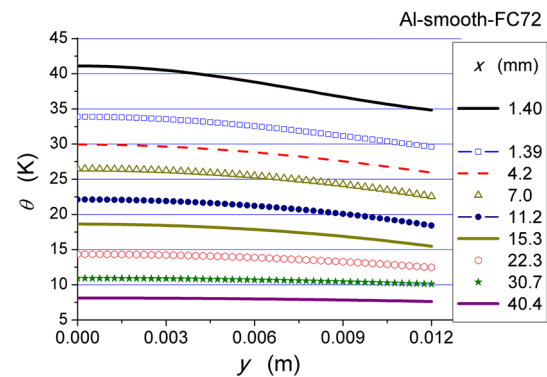
a greater thickness, e.g. 12 mm, the temperature changes through the thickness cannot be neglected while determining the heat transfer conditions. The Biot number for the 12 mm thick fin is about 0.32, so the problem must be at least two-dimensional. Systems with an easy-to-observe surface can have the thermal field measured; the boiling heat transfer coefficient can be calculated using the algorithm described in Sect. 3.2. For the distribution of temperature measured at the fin surface (Fig. 3), it was essential to assume the boundary conditions (5)–(8), develop an approximation of  $\Theta(x,y)$ , and calculate the coefficients  $c_j$  from the best fit condition. The function determined in this way describes the thermal field in the OABC area (see Fig. 4).

Figure 8 presents the measured and calculated values of the wall superheat for two surfaces of the 12 mm thick fin, i.e.  $y = 0$  and  $y = h$  (see Fig. 4). By comparison, during boiling heat transfer, e.g. by natural convection or by forced convection with no phase change, large amounts of heat flux are removed. The largest are in the nucleate boiling regime. As shown in Fig. 7, for the smooth aluminium sample with a thickness of 12 mm, the process starts at a wall superheat of about 8 K at a distance of about 3 cm from the base (see Fig. 8). With a rise in the wall superheat in the nucleate boiling regime, there is an increase in the heat transfer coefficient. Heat flux removal increases locally, resulting in an increase in the difference in temperature between the outer surface ( $y = 0$ ) and the inner surface ( $y = h$ ). The value exceeds 5 K at points located near the base of the 12 mm thick fin. This fact cannot be ignored in the analysis of heat transfer in fins with such a geometry.

Figure 9 shows a gradient of the wall superheat over the outer surfaces ( $y = 0$  and  $y = h$ ) along the fin length. The calculated values result from the assumed boundary conditions. It should be noted that a good convergence of the measurement results with the assumed values is found.



**Fig. 9** Temperature gradients along the fin length



**Fig. 10** Temperature distribution at different cross-sections of the fin

However, some disagreement with Eq. 7 is observed for the temperature at the base of the fin. As can be seen from Fig. 10, the distribution of the wall superheat for  $x = 0$  changes with the height. The variability of this quantity is a result of a very high heat transfer coefficient, and it seems to correct the assumed boundary condition.

Figure 10 shows the numerically calculated distribution of temperature in the 12 mm thick fin in selected cross-sections. There is a significant change in temperature in the fin cross section to the height of about 30 mm from the base. Near the surface, where nucleate boiling exists, the temperature drops considerably. Beyond this area, the decrease in temperature is insignificant.

In the numerical calculations, the approximation of the exact solution (13) is employed to determine the thermal field, which can be used to calculate the temperature gradients. In accordance with the Fourier law, this gradient, multiplied by the coefficient of heat conductivity, determines the heat flux density. On the other hand, the one calculated in the perpendicular direction on the inner edge ( $y = h$ ) is equal to the boiling heat transfer on the fin:

$$q_\alpha = -\lambda \left. \frac{\partial \Theta}{\partial y} \right|_{y=h} \quad \text{and} \quad \alpha = \frac{q_\alpha}{\Theta} \quad (19)$$

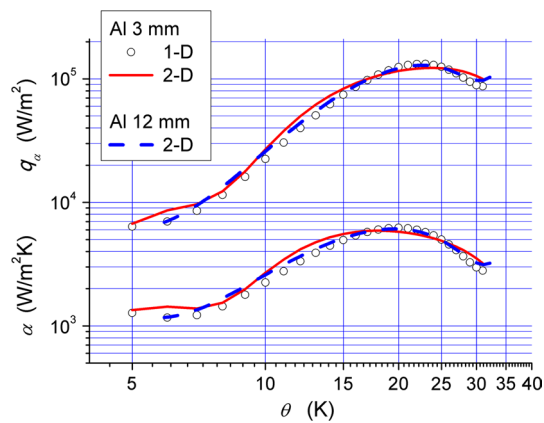


**Fig. 11** Boiling curve for FC 72 at ambient pressure on an aluminium fin

The calculation result in the perpendicular direction on the inner edge ( $y = h$ ) of the fin is presented in the form of a boiling curve in Fig. 11.

The boiling curve is defined locally, i.e. for the local values of heat flux and heat transfer coefficients from wall superheat. The temperatures are taken at the inner surfaces of the fins. For the 3 mm thick fin, the temperature values at the inner and outer surfaces are nearly the same. For the thicker fin, the difference is significant, as shown in Figs. 8 and 10. The total heat dissipation for the two fins is given in Figs. 2 and 3, respectively.

The analysis of heat transfer for refrigerant FC 72 boiling at ambient pressure over an aluminium fin shows that two steady boiling regimes on the surface: nucleate boiling and free convection are found. The boiling curve can be divided into three characteristic regimes. In the low superheat regime (up to about 6.5 K), free convection at a nearly constant value of the heat transfer coefficient is observed. In the range of the wall superheat higher than 7 K, two subregimes can be distinguished. When the wall superheat is in the range from about 7 K to  $\sim 8.5$  K, single bubbles lift off the surface and cause more intensive mixing of the fluid close to the fin surface. When the wall superheat grows above 9 K, more nucleation sites become active and the nucleation boiling regime occurs. As a result, a rapid rise in the heat flux density and the heat transfer coefficient is observed.

Due to the very high coefficient of heat transfer in the nucleate boiling regime, in order to ensure a good representation of one-dimensional heat conduction, it is necessary to prepare the fin of a material with high thermal conductivity and low thinness. Both of those affect the value of the Biot number, which should be as small as possible. Therefore, studies were performed for aluminium fins with a thickness of 3 mm, for which at the maximum heat transfer coefficient,  $Bi \approx 0.08$  and gradually decreases with drop of the local heat transfer coefficient.

Figure 6a shows the wall superheat along the height of the fin. The figure presents measurement result and two lines for  $y = 0$  and  $y = h$ , which were determined numerically by the given algorithm. From the comparison of the temperature difference from the side of thermovision camera shown in Fig. 6b, the errors of the method could be drawn out. From the set under consideration, it can be seen that almost all values are within the range  $\pm 0.2$  K and the standard deviation equals 0.102 K.

For the fin made of aluminium with a thickness of 12 mm, temperature distribution in its cross OABC was calculated (see Fig. 4), and the results are shown in Figs. 8 and 10. Temperature difference between inner and outer surfaces at the base of the fin is considerable and reaches slightly above 5.5 K. The difference of these values below 0.5 K occurs only at a distance greater than 35 mm from the base, where free convection boiling is observed.

Figure 9 shows the temperature gradients. Its value in the direction of the  $y$ -axis is almost zero, which indicates the correct adoption of the boundary condition (6). The other two curves in this figure are the result of good agreement of measured and calculated temperatures at the surface, as discussed above.

For the commercial surface with lots of microcavities, the nucleate boiling regime starts at a wall superheat of about 9 K and, as more nucleation sites become active, and grows rapidly with the superheat increase, as shown in the boiling curve in Fig. 11. For superheat above 8 K, the heat transfer coefficient gradually increases and its maximum is about  $\sim 6.2$  kW/m<sup>2</sup>K at the wall superheat of 20 K. The increased generation of vapor causes bubble interference and coalescence, and the vapour escapes in forms of jets or columns, which subsequently merge into slugs. This is accompanied by a much slower increase in the heat transfer coefficient and at the wall superheat above  $\sim 23.5$  K, a consequent decrease in the heat flux density is observed.

## 6 Conclusions

The aim of the experimental research was to measure the local values of the heat flux and the boiling heat transfer coefficient on a non-isothermal fin surface. The thermal conductivity of aluminium under nucleate boiling conditions is relatively high, but 12 mm thickness of the fin makes the Biot number much higher than 0.1.

The study involved comparing two fins with the same surface morphology but different thicknesses. For the thinner fin, the Biot number was smaller than 0.1, while for the thicker fin the number was much greater. The boiling curves plotted for the two specimens in accordance with the 1-D procedure described in Sect. 2.1 are clearly different from each other in shape and value (see Fig. 7). The

maximum difference is more than 31 % at a wall superheat of 18 K.

Since it is impossible to use a 1-D model of heat transfer for such a system, the calculations were conducted using a two-dimensional heat conduction equation, which is an ill-conditioned problem due to the measurement method applied.

To validate the method of calculation, a series of measurements was performed, whose purpose was to estimate the local heat transfer coefficient under conditions as close as possible to one-dimensional temperature distribution and to compare those results with the analogous ones obtained using the method in the inverse problem.

The performance of 1-D fin with a constant cross-section is analysed on the basis of a one-dimensional expression for the temperature distribution. With an assumption that the outcome of integration is an holomorphic function, its value is represented by a power series. By differentiating this expression, functional dependences for the local heat fluxes and heat transfer coefficients are obtained. In this way the corresponding boiling curve for the investigated surface is given and thoroughly discussed in the paper.

The results of numerical calculations are the temperature values inside the area and on the invisible side (see Fig. 10). They are described by the formula (13). On this basis, the local heat flux density and corresponding heat transfer coefficient are evaluated, as shown in Figs. 7 and 11. There, a correlation between the values calculated assuming a one-dimensional model of heat transport phenomena in the fin is also presented. Visible reduction in heat transfer coefficient in the high heat fluxes range is the result of polynomial approximation used in the model 1-D and cannot be here the basis for inference about the location of the first critical point of boiling.

The approximation of the test results shown in Fig. 5 was performed with sixth degree polynomial. Eq. (3) was used to determine the local heat flux or the heat transfer coefficient:

$$\alpha = \frac{q_\alpha}{\theta} = a_0 + a_1\theta + a_2\theta^2 + a_3\theta^3 + a_4\theta^4 + a_5\theta^5. \quad (20)$$

The coefficients were as follows:  $a_0 = 5470.05 \text{ W/m}^2\text{K}$ ,  $a_1/a_0 = -0.30757 \text{ K}^{-1}$ ,  $a_2/a_0 = 0.034797 \text{ K}^{-2}$ ,  $a_3/a_0 = -0.00094 \text{ K}^{-3}$ ,  $a_4/a_0 = -9.3\text{E} - 06 \text{ K}^{-4}$ ,  $a_5/a_0 = 4.24\text{E} - 07 \text{ K}^{-5}$  (valid in the range of  $\theta = 6\text{--}31 \text{ K}$ ).

To sum up, the analysis performed shows that the proposed method provides accurate results coincident with 1D ones. The obtained results of this study show that the method proposed is accurate and efficient for solving the engineering heat transfer problems where the thermal field could be measured and corresponding heat fluxes are sought.

**Open Access** This article is distributed under the terms of the Creative Commons Attribution 4.0 International License (<http://creativecommons.org/licenses/by/4.0/>), which permits unrestricted use, distribution, and reproduction in any medium, provided you give appropriate credit to the original author(s) and the source, provide a link to the Creative Commons license, and indicate if changes were made.

## References

1. Dhir VK (1998) Boiling heat transfer. *Annu Rev Fluid Mech* 30:365–401
2. Ahn HS, Kim M, Kaviany M, Kim MH (2014) Pool boiling experiments in reduced graphene oxide colloids. Part I—boiling characteristics. *Int J Heat Mass Transf* 74:501–512
3. Ahn HS, Kim M, Kaviany M, Kim MH (2014) Pool boiling experiments in reduced graphene oxide colloids. Part II—behavior after the CHF, and boiling hysteresis. *Int J Heat Mass Transf* 78:224–231
4. Naphon P, Thongjirakul C (2014) Pool boiling heat transfer characteristics of refrigerant-nanoparticle mixture. *Int Commun Heat Mass Transf* 52:84–89
5. Ahn HS, Kim MH (2013) The boiling phenomenon of alumina nanofluid near critical heat flux. *Int J Heat Mass Transf* 62:718–728
6. Piro IL (1999) Experimental evaluation of constants for the Rohsenow pool boiling correlation. *Int J Heat Mass Transf* 42:2003–2013
7. Piro IL, Rohsenow W, Doerfer SS (2004) Nucleate pool-boiling heat transfer. II: assessment of prediction methods. *Int J Heat Mass Transf* 47:5045–5057
8. Kolev NI (1995) How accurately can we predict nucleate boiling? *Exp Therm Fluid Sci* 10:370–378
9. Adib TA, Vasseur J (2008) Bibliographic analysis of predicting heat transfer coefficients in boiling for applications in designing liquid food evaporators. *J Food Eng* 87:149–161
10. Shah MM (2005) Evaluation of general correlations for heat transfer during boiling of saturated liquids in tubes and annuli. ASME summer heat transfer conference USA, HT2005-72025
11. Orzechowski T, Tyburczyk A (2013) Heat transfer on fins operating at boiling—experimental and numerical procedure. In: EPJ web of conferences: experimental fluid mechanics 2013 pp 523–529
12. Roh H-S (2014) Heat transfer mechanisms in pool boiling. *Int J Heat Mass Transf* 68:332–342
13. Orzechowski T (2001) Analysis of the boiling heat transfer from a microstructure-covered fin. *Arch Thermodyn* 22:77–94
14. Krikkis R, Sotirchos SV, Razelos P (2004) Analysis of multiplicity phenomena in longitudinal fins under multi-boiling conditions, ASME. *J Heat Transf* 126:1–7
15. Liaw S-P, Yeh R-H, Yeh W-T (2005) A simple design of fins for boiling heat transfer. *Int J Heat Mass Transf* 48:2493–2502
16. Gonzalez-Fernandez CF, Alarcon MF, Alhama F (2004) Transient multibooling in a pin fin with temperature dependent thermal conductivity. *Heat Mass Transfer* 41:67–74
17. Turkyilmazoglu M (2012) Exact solutions to heat transfer in straight fins of varying exponential shape having temperature dependent properties. *Int J Therm Sci* 55:69–75
18. Kundu B, Lee K-S (2012) Analytic solution for heat transfer of wet fins on account of all nonlinearity effects. *Energy* 41:354–367
19. Taler J (1988) A general method for the experimental determination of local transient heat transfer coefficients. *Wärme- und Stoffübertragung* 23:283–289

20. Chen H-T, Lai S-T, Haung L-Y (2013) Investigation of heat transfer characteristics in plate-fin heat sink. *Appl Therm Eng* 50:352–360
21. Torabi M, Aziz A (2012) Thermal performance and efficiency of convective–radiative T-shaped fins with temperature dependent thermal conductivity, heat transfer coefficient and surface emissivity. *Int Commun Heat Mass Transf* 39:1018–1029
22. Konda Reddy B, Balaji C (2012) Estimation of temperature dependent heat transfer coefficient in a vertical rectangular fin using liquid crystal thermography. *Int J Heat Mass Transf* 55:3686–3693
23. Diez LI, Espatolero S, Cortés C, Campo A (2010) Thermal analysis of rough micro-fins of variable cross-section by the power series method. *Int J Therm Sci* 49:23–35
24. Huang C-H, Chang W-L (2012) An inverse design method for optimizing design parameters of heat sink modules with encapsulated chip. *Appl Therm Eng* 40:216–226
25. Grysa K, Maciąg A, Pawinska A (2012) Solving nonlinear direct and inverse problems of stationary heat transfer by using Trefftz functions. *Int J Heat Mass Transf* 55:7336–7340
26. Das R, Mallick A, Ooi KT (2013) A fin design employing an inverse approach using simplex search method. *Heat Mass Transf* 49:1029–1038
27. Zueco J, Alhama F, González Fernández CF (2005) Numerical nonlinear inverse problem of determining wall heat flux. *Heat Mass Transf* 41:411–418
28. Orzechowski T (2007) Determining local values of the heat transfer coefficient on a fin. *Exp Therm Fluid Sci* 31:947–955
29. Ciałkowski M, Frąckowiak A (2000) Heat functions and their application to solving heat conduction and mechanical problems. Poznań University of Technology, Poznań (**in Polish**)